

Landau quantization in buckled monolayer GaAs

Hsien-Ching Chung* and Chih-Wei Chiu†

Department of Physics, National Kaohsiung Normal University, Kaohsiung 824, Taiwan

Chun-Nan Chen

*Quantum Engineering Laboratory, Department of Physics,
Tamkang University, Tamsui, New Taipei 25137, Taiwan*

Ming-Fa Lin‡

Department of Physics, National Cheng Kung University, Tainan 70101, Taiwan

(Dated: September 12, 2021)

Magneto-electronic properties of buckled monolayer GaAs is studied by the developed generalized tight-binding model, considering the buckled structure, multi-orbital chemical bondings, spin-orbit coupling, electric field, and magnetic field simultaneously. Three group of spin-polarized Landau levels (LLs) near the Fermi level are induced by the magnetic quantization, whose initial energies, LL degeneracy, energy spacings, magnetic-field-dependence, and spin polarization are investigated. The Landau state probabilities describing the oscillation patterns, localization centers, and node regularities of the dominated/minor orbitals are analyzed, and their energy-dependent variations are discussed. The given density of states directly reflects the main features of the LL energy spectra in the structure, height, number, and frequency of the spin-polarized LL peaks. The electric field causes the monotonous/nonmonotonous LL energy dispersions, LL crossing, gap modulation, phase transition and spin splitting enhancement. The complex gap modulations and phase transitions based on the competition between magnetic and electric fields are explored in detail by the phase diagram. The field-controlled gap modulations and phase transitions are helpful in designing the top-gated and phase-change electronic devices. These predicted magneto-electronic properties could be verified by scanning tunneling spectroscopy measurements.

I. INTRODUCTION

Over the past decade, graphene [1, 2] has successfully brought scientists into the world of two-dimensional (2D) materials based on its incredible intrinsic properties, such as high carrier mobility at room temperature ($> 200000 \text{ cm}^2/\text{Vs}$) [3–5], superior thermoconductivity ($3000\text{--}5000 \text{ W/mK}$) [5, 6], high transparency for incident light over a wide range of wavelength (97.7 %) [7, 8], extremely large modulus ($\sim 1 \text{ TPa}$) and tensile strength ($\sim 100 \text{ GPa}$) [9]. Few-layer graphene are observed to have diverse magnetic quantizations, e.g., the Landau levels (LLs) with $\sqrt{B_z}$ -dependence in monolayer graphene featuring massless Dirac fermion [10–14], the LLs with linear B_z -dependence in AB-stacked bilayer graphene featuring massive Dirac fermion [15–17], as well as the coexistence of square-root and linear B_z -dependent LLs in graphene of trilayer ABA stacking [18], where B_z is the strength of magnetic field. Although interest in graphene is still high, it is also conspicuous that graphene has its limitation. For instance, in contrast to conventional semiconductors, the lack of a significant band gap limits its applicability in electronics where high transistor on/off ratios are vital [19]. This obstacle triggers researches on emergent 2D materials [20–22], covering group-IV [23–25],

group-V [26–28], group III-V compounds [29–31], and transition-metal dichalcogenides (TMDs) [32–35]. Such 2D layered materials are expected to have the rich and essential properties, being sensitive to the lattice symmetry, stacking configuration, layer number, orbital hybridization, spin-orbit coupling (SOC), as well as external electric and magnetic fields. This work is focused on the magnetic quantization of monolayer GaAs using the generalized tight-binding model. Comparisons to graphene are also made.

Group-IV monoelemental 2D honeycomb materials beyond graphene, such as silicene, germanene, and stanene, have been proposed to possess a band gap owing to SOC [36–38]. Recently, few-layer silicene, germanene, and stanene have been synthesized on various substrates: silicene on Ag(111) [39–42], Ir(111) [43], and ZrB₂(0001) [44]; germanene on Pt(111) [45], Al(111) [46], and Au(111) [47]; stanene on Bi₂Te₃(111) [48]. Silicene, germanene, and stanene having buckled structure with SOC, which grow as the atomic mass increases, are much different from the planar hexagonal graphene without SOC. Their low-energy electronic structures are dominated by the SOC and the hybridization of multi-orbitals. The group-IV materials with heavy atomic masses have broad buckled angle and strong SOC, leading to a large gap, e.g., the gap of germanene (stanene) is comparable to (larger than) the thermal energy at room temperature [37, 49]. Moreover, magnetic quantizations with various magnetic-field-dependent LLs and monotonous/nonmonotonous electric-field-

* E-mail: hsienching.chung@gmail.com;

Homepage: <https://sites.google.com/site/hsienchingchung/home>

† E-mail: giorgio@fonran.com.tw

‡ E-mail: mflin@mail.ncku.edu.tw

dependent LLs with subband crossing/anticrossing are predicted [50–54]. However, the strong interactions between silicene (germanene, or stanene) and substrate deform the buckled structure and mix the electronic states of silicene and substrate near the Fermi level, making the modification of low-energy electronic properties. Recent experiments on tunneling spectra of silicene closing to the liquid-helium temperature have evidenced the disappearance of LL sequences based on the instability from the dangling bonds of the sp^3 -hybridized atoms [55].

Apart from 2D materials of group-IV elements, the binary compounds of group III-V elements have also been proposed as honeycomb lattices with large gaps [29–31]. Although the group III-V elemental 2D materials of buckled structure with mixed sp^3 – sp^2 bonding are more stable compared to those of planar ones with sp^2 bonding [29], the dangling-bond-induced instability remains. A promising route is to saturate the dangling bonds by halogen atoms, which has been used in graphene [56–58]. First-principles calculations indicate that iodinated germanene (GeI) [59] and fluorinated stanene (SnF) [38] are free from dangling bonds and interact weakly with substrates. Their gaps are about 0.3 eV at the Γ point, considerably larger than the values of the unpassivated 2D systems. Bulk GaAs is one of the famous group III-V elemental binary compounds, being widely used in the manufacture of electronic and optical devices due to its direct band gap (silicon is indirect gap) and high mobility (than silicon) [60, 61]. According to first-principles calculations [62], monolayer GaAs possesses buckled hexagonal structure, multi-orbital chemical bonding, and significant SOC, leading to rich electronic properties. This system will exhibit diverse magnetic quantization in the presence/absence of electric fields.

The generalized tight-binding model built from the subenvelope functions on the layered-dependent distinct sublattices is developed to study the electronic properties under uniform/non-uniform external electric and magnetic fields. The geometric structures, multi-orbital hybridizations, SOC, and external fields are included in the calculation, simultaneously. The quantized energy spectra and wave functions can be efficiently computed by the method of exact diagonalization even for a rather large Hamiltonian with complex matrix elements. This model has been widely adopted to make systematic studies on multi-dimensional carbon-based materials and hybrid systems, ranging from three-dimensional (3D) graphites [63–65], 2D graphenes [63, 66–70], 1D graphene nanoribbons (GNRs) [71–76], carbon nanotubes (CNTs) [77–82], graphene nanoflake [83] and graphene-related hybrids [84]. It is also suitable for studying the mainstream layered materials, such as group-IV [53, 54, 85, 86], group-V [87–90], and TMD [91–96] 2D materials.

In this work, buckled monolayer GaAs with each atom being passivated by a F atom is chosen as a model study [Fig. 1(a)]. The dangling bonds are saturated, and thus the effects of substrate can be elimi-

nated. The generalized tight-binding model, simultaneously considering geometric structure, multi-orbital hybridization, SOC, and external fields, is employed to explore the magneto-electronic properties. The low-lying electronic structure is composed of a direct energy gap and three groups of SOC-induced spin-polarized subbands presenting monotonous energy dispersions with strong wavevector-dependent (\mathbf{k} -dependent) spin splitting. The state probabilities giving the detailed informations about the dominated/minor orbitals of each subband and their \mathbf{k} -dependent variations are discussed. Magnetic quantization, accumulating electronic states with similar energies, induces three groups of LLs. The initial energy of each LL group, subband degeneracy, energy spacing among LLs, and spin polarization are investigated. The LL state probabilities, whose oscillation patterns are similar to those of harmonic oscillators with regular nodes at the localization centers, are analyzed. The complex variation of LL dominated/minor orbitals are observed to reflect the average of accumulated neighboring zero-field electronic states. It is predicted that the LL energies have the linear- B_z dependence with the enhancement of spin splitting for an increasing magnetic field. The given density of states (DOS) directly reflects the main features of the LL energy spectra in the structure, height, number, and frequency of the three-group spin-polarized LL peaks. The electric field, contributing to an electric potential difference in the buckled structure, gives rise to monotonous/nonmonotonous energy dispersions, LL crossing, gap modulation, and enhancement of spin splitting. The complex gap modulations and phase transitions based on the competition between magnetic and electric fields are investigated in detail. A phase diagram about the complex phase transitions between four characteristic regions is illustrated, presenting that the external-fields-controlled gap presents several types of modulation, associated to different region-to-region phase transitions. A brief comparison between the buckled monolayer GaAs and planer graphene is described for the differences in essential properties and responses to external fields based on the orbital domination, SOC, and geometric structure. The predicted magneto-electronic properties of the monolayer GaAs, including three groups of spin-polarized LL DOS peaks with linear B_z -dependence, SOC-induced spin splitting, the external-field-controlled gap modulation/phase transition, electric-field-enhanced spin splitting, could be identified by scanning tunneling spectroscopy (STS) measurements. Furthermore, this work can serve as a model study for understanding magnetic quantizations of other group III-V 2D materials.

II. GENERALIZED TIGHT-BINDING MODEL

Monolayer GaAs has the buckled honeycomb lattice with each atom being passivated by a F atoms [Fig. 1(a)]. Both sp^3 -hybridized Ga and As atoms bond to four atoms

(three for As or Ga; one for F) and the Ga-As bond length is about 2.521 Å. A unit cell containing two different Ga and As sublattices is indicated by the rhombus with the primitive unit vectors, \mathbf{a}_1 and \mathbf{a}_2 of a lattice constant $a = 4.226$ Å. The altitude of the buckled structure measured from the distance between the Ga-plane and As-plane is $l_z = 0.633$ Å [Fig. 1(b)]. The buckling angle θ between the Ga-As bond and the z -axis is about 104.54° . This configuration is free from dangling bonds and thus chemically stable [62].

To illustrate the electronic properties explicitly, the Hamiltonian built from the tight-binding functions of $4s$, $4p_x$, and $4p_y$ orbitals is expressed as

$$\mathcal{H} = \sum_{m,\alpha} \epsilon_m^\alpha c_m^{\alpha\dagger} c_m^\alpha + \sum_{\langle m,n \rangle, \alpha, \beta} \gamma_{mn}^{\alpha\beta} (c_m^{\alpha\dagger} c_n^\beta + h.c.), \quad (1)$$

where ϵ_m^α , $c_m^{\alpha\dagger}$, and c_m^α respectively represent the on-site energy, creation, and annihilation operators of an electron at the α -orbital of the m -th atom. $\gamma_{mn}^{\alpha\beta}$ is the nearest-neighbor hopping integral between an α -orbital of the m -th atom and a β -orbital of the n -th atom. The multi-orbital hopping integrals are $\gamma_{mn}^{ss} = V_{ss\sigma}$, $\gamma_{mn}^{sp_x} = V_{sp\sigma} \cos \theta_x$, $\gamma_{mn}^{sp_y} = V_{sp\sigma} \cos \theta_y$, $\gamma_{mn}^{p_x p_x} = V_{pp\sigma} \cos^2 \theta_x + V_{pp\pi} (1 - \cos^2 \theta_x)$, $\gamma_{mn}^{p_y p_y} = V_{pp\sigma} \cos^2 \theta_y + V_{pp\pi} (1 - \cos^2 \theta_y)$, and $\gamma_{mn}^{p_x p_y} = (V_{pp\sigma} - V_{pp\pi}) \cos \theta_x \cos \theta_y$, where θ_x and θ_y are respectively the angles of the vector pointed from the m -th atom to the n -th atom with respect to the x - and y -axis [97], and the Slater-Koster hopping parameters in the sp^3 bonding optimized at the equilibrium state are $V_{ss\sigma} = -1.707$ eV, $V_{sp\sigma} = 2.056$ eV, $V_{pp\sigma} = 2.650$ eV, and $V_{pp\pi} = -0.827$ eV [62]. The on-site energies of s - and p -orbitals are set to the values (-12.00 eV, -5.67 eV) for Ga and (-17.68 eV, -8.30 eV) for As, being taken from those of bulk GaAs [98].

When an electron with momentum \mathbf{p} moving close to the atomic nuclei in a crystal with potential V , it experiences an effective magnetic field $B_{\text{eff}} \sim \nabla V \times \mathbf{p}/m_0 c^2$ in its rest-frame (m_0 is the mass of a free electron and c is the speed of light). Such field induces a momentum-dependent Zeeman energy called the SO coupling, which is given by

$$H^{SO} = \frac{\hbar}{4m_0^2 c^2} (\nabla V \times \mathbf{p}) \cdot \boldsymbol{\sigma}, \quad (2)$$

where \hbar is the reduced Planck constant and $\boldsymbol{\sigma}$ is the vector of Pauli matrices. In the central field approximation, the crystal potential $V(\mathbf{r})$ is considered as the spherical atomic potential. The SOC term on the same atom is taken into account and it can be obtained by calculating the mean value:

$$H_{i,\alpha\beta}^{SO} = \lambda_i \langle \mathbf{L} \cdot \boldsymbol{\sigma} \rangle_{\alpha\beta}, \quad (3)$$

where λ_i is the SOC strength of the i -th atom and \mathbf{L} is the orbital angular momentum operator. The matrix element $\langle \mathbf{L} \cdot \boldsymbol{\sigma} \rangle_{\alpha\beta}$ is given in the basis of atomic orbitals (α, β), and the dimensionless SOC operator $\mathbf{L} \cdot \boldsymbol{\sigma}$ for the

relevant orbitals ($4s$, $4p_x$, and $4p_y$) in the 2D system is given by

$$\mathbf{L} \cdot \boldsymbol{\sigma} = \begin{pmatrix} 0 & 0 & 0 \\ 0 & 0 & -is_z \\ 0 & is_z & 0 \end{pmatrix}, \quad (4)$$

where $s_z = \begin{pmatrix} 1 & 0 \\ 0 & -1 \end{pmatrix}$. The SOC strengths of Ga and As atoms are chosen to be 0.058 eV and 0.140 eV, respectively [99].

When a uniform perpendicular magnetic field, $\mathbf{B} = B_z \hat{z}$, is applied to monolayer GaAs, the effective Hamiltonian can be regarded as the Peierls substitution Hamiltonian [100]. Each Hamiltonian matrix element turns into the product of the zero-field element and the extra Peierls phase, $\exp(i2\pi\theta_{mn})$, where $\theta_{mn} = (1/\phi_0) \int_m^n \mathbf{A} \cdot d\mathbf{l}$ is a line integral of the vector potential \mathbf{A} from the m -th to n -th site, \mathbf{A} is chosen as $(0, B_z x, 0)$ in the Landau gauge, and $\phi_0 = h/e$ (4.1357×10^{-15} T·m²) is the magnetic flux quantum [101, 102]. The unit cell becomes an enlarged rectangle with $2R_B$ Ga and $2R_B$ As atoms to satisfy the periodicity of Peierls phase, where $R_B = \phi_0/\phi = \phi_0/(B_z \sqrt{3}/2a^2) \sim 26739$ T/ B_z is the ratio of flux quantum to magnetic flux through a hexagon ϕ [Fig. 2(a)]. The reduced Brillouin zone has an area of $4\pi^2/\sqrt{3}a^2 R_B$. The Hamiltonian is built in the space spanned by the $24R_B$ tight-binding functions $\{|Ga_m^{orb}\rangle, |As_m^{orb}\rangle; m = 1, 2, 3, \dots, 2R_B; orb = 4s, 4p_x, 4p_y\} \otimes \{\uparrow, \downarrow\}$. An electric field $\mathbf{E} = E_z \hat{z}$ along the z -axis introduces a potential energy $-eE_z l_z/2$ ($eE_z l_z/2$) to the site energy of the Ga (As) sublattice. The exact diagonalization of the Hamiltonian matrix \mathcal{H} yields the energy spectrum $E^{c,v}$ and wave functions $|\Psi^{c,v}\rangle$, where the superscripts c and v denote the conduction and valence subbands, respectively. The generalized tight-binding model can be further developed to comprehend the Landau quantization in other layered systems with complex orbital bondings and spin configurations.

III. SPIN-POLARIZED MAGNETO-ELECTRONIC PROPERTIES

Monolayer GaAs has feature-rich energy bands, mainly owing to the low-buckled structure, sp^3 bonding, and SOC. There exist three low-lying energy subbands, i.e., the unoccupied conduction subband (n_1) and two occupied valence subbands (n_2 and n_3) with different curvatures near the Γ point, touching at the Fermi level ($E_F = 0$). Without the SOC, they have the strong wavevector-dependence in the monotonous form [dashed curves in Fig. 1(c)]. Each subband is two-fold degenerate for the spin degree of freedom except that the n_2 and n_3 subbands intersect and possess a four-fold degeneracy. The conduction and valence subbands near the Γ point are respectively dominated by the $4s$ and ($4p_x, 4p_y$) orbitals [62]. More importantly, a direct band gap of

$E_g = 0.742$ eV is determined by the band-edge states of n_1 and n_2/n_3 at the Γ point. The significant SOC further induces the variation of band gap and spin splitting [solid curves in Fig. 1(c)]. The band gap shrinks to $E_g^{SO} = 0.623$ eV, while the n_2 and n_3 valence subbands are separated by $\Delta_{SO} = 0.237$ eV, lifting the state degeneracy at the Γ point from four- to two-fold. The spin degeneracy is removed except for the zone from the Γ point to the M point. Therefore, the spin-degenerate subbands become spin-polarized subbands. The splitting energies between spin-up and spin-down subbands gradually increase when deviating from the Γ point and reach maxima at the K (K') points (e.g., 0.196 eV between n_1^\uparrow and n_1^\downarrow subbands; 0.133 eV between n_2^\uparrow and n_2^\downarrow subbands). Such spin splitting has also been found in GaAs quantum wells by photocurrent measurements [103], where SOC leads to terms linear in wavevector \mathbf{k} in the effective Hamiltonian [104].

The state probability ($|\Psi^{c,v}|^2$) exhibits the spacial contribution of different orbitals on subbands and figures out the variations of dominated/minor orbitals near various high-symmetric points. A whole range of the orbital variation on different sublattices for the n_1^\uparrow , n_2^\uparrow , and n_3^\uparrow subbands is shown in Figs. 1(d)–(o). It is sufficient to discuss one of the polarized states (e.g., spin-up states) because the state configurations of spin-up (white zones) and spin-down (gray zones) states are quite similar. The state probabilities for different orbitals are very sensitive to the sublattices and wavevectors. In the conduction n_1^\uparrow and valence n_3^\uparrow subbands, the s -orbitals (red curves) and p_x -orbitals (green curves) are respectively the most dominated contributions on the Ga and As sublattices for a wide range of \mathbf{k} . The p_y -orbitals (blue curves) are the dominated contributions in the valence n_2^\uparrow subbands. Remarkably, the p_x - and p_y -orbitals on a specific sublattice are of identical intensity at the high-symmetric Γ and K points. The state probabilities near the Γ point, which are much different from the probabilities far away the Γ point, reveal the orbital variation for the low-lying states. The conduction subbands are dominated by the s -orbitals, whose state probabilities on the Ga sublattice is larger than those on the As sublattice [Figs. 1(d)–(g)]. The increase of p_x - and p_y -orbital strength and the decrease of s -orbital strength arise as \mathbf{k} deviates from the Γ point. The valence n_2 (n_3) subbands are dominated by p_y -orbitals (p_x -orbitals) [Figs. 1(h)–(o)]. Instead of the Ga sublattices, the dominated orbitals on the As sublattices possess larger strength. It should be noted that the relative strength of the orbital probabilities for the low-lying states will reflect on the quantized magneto-electronic states. In other words, the low-energy Landau states features those accumulated zero-field states near the Γ point (discussed later).

Magnetic fields constrain carrier motions in real space, bring neighboring electronic states together, and induce highly degenerate Landau states. Near the Fermi energy, there are three groups of spin-polarized dispersion-

less LLs, i.e., one group of occupied conduction LLs [n_1^\uparrow and n_1^\downarrow in Fig. 2(b)] and two groups of unoccupied valence LLs [n_2^\uparrow , n_2^\downarrow , n_3^\uparrow , and n_3^\downarrow in Figs. 2(e) and (f)]. The distinct spin polarization in each group of LLs results from the SOC between the $4p_x$ and $4p_y$ orbitals. Their LL initial energies are respectively near 0.62 eV, 0 eV, and -0.24 eV, which reflect the energies of electronic states at the Γ point in the absent of magnetic fields. For each (k_x, k_y) , all LLs are two-fold degenerate, being attributed to the one Γ -valley degree of freedom and the mirror symmetry of $z = 0$ plane. As the state energy grows, the energy spacing between LLs of the same spin-up (or spin-down) subgroup gradually shrinks.

Wave functions, presenting the spatial information of electronic states, are very important in realizing fundamental physical properties, such as charge densities [105–108], state mixing [109, 110], and optical selection rules [75, 76, 111, 112]. Under the influence of magnetic fields, wave functions in monolayer GaAs present peculiar spatial distributions, where the localization center, orbital domination, waveform, and node number are very sensitive to the wavevector, state energy, and spin polarization. Each spin-polarized LL wave function can be decomposed into subenvelope functions with the (s, p_x, p_y) orbitals on the Ga and As sublattices at the odd and even sites. For the sake of simplicity, only the distribution probabilities of subenvelope functions at the odd sites (Ga_o and As_o) will be considered because the even-site probabilities have the same behavior as the odd-site ones. The localization centers of the LL wave functions are strongly dependent on the wavevector. At $(k_x, k_y) = (0, 0)$, one of the doubly degenerate spin-polarized LL states is localized at the $1/2$ position of the enlarged unit cell ($m/2R_B = 1/2$) and the other is localized at the 0 position. The Landau states at the $1/2$ position are chosen for illustrating the main features, since the state probabilities at 0 and $1/2$ positions only differ in the localization center. The probabilities of subenvelope functions are well-behaved in their spatial distributions. Their oscillation patterns at the localization center are similar to those of harmonic oscillators, having regular node (zero-point) numbers. For any particular LL, the node numbers of various orbital subenvelope functions are identical for the Ga and As sublattices. The dominated-orbital subenvelope function is significant for characterizing the Landau state, and its node number, which gradually grows as the state energy increases, is appropriate for labeling the LL. In the n th conduction LLs ($n_1^\uparrow = n$ and $n_1^\downarrow = n$), the probabilities of dominated s -orbital subenvelope functions with n nodes have strength larger than the probabilities of minor (p_x and p_y)-orbital subenvelope functions with $n + 1$ nodes [Figs. 2(c) and (d)]. In the $n_2^\uparrow = n$ ($n_2^\downarrow = n$) valence LLs, there are n , n , and $n + 1$ ($n - 1$) nodes in the dominated p_y -orbitals and minor p_x - and s -orbitals, respectively [Figs. 2(g) and (h)]. In the $n_3^\uparrow = n$ ($n_3^\downarrow = n$) valence LLs, n , n , and $n - 1$ ($n + 1$) nodes are respectively in the dominated

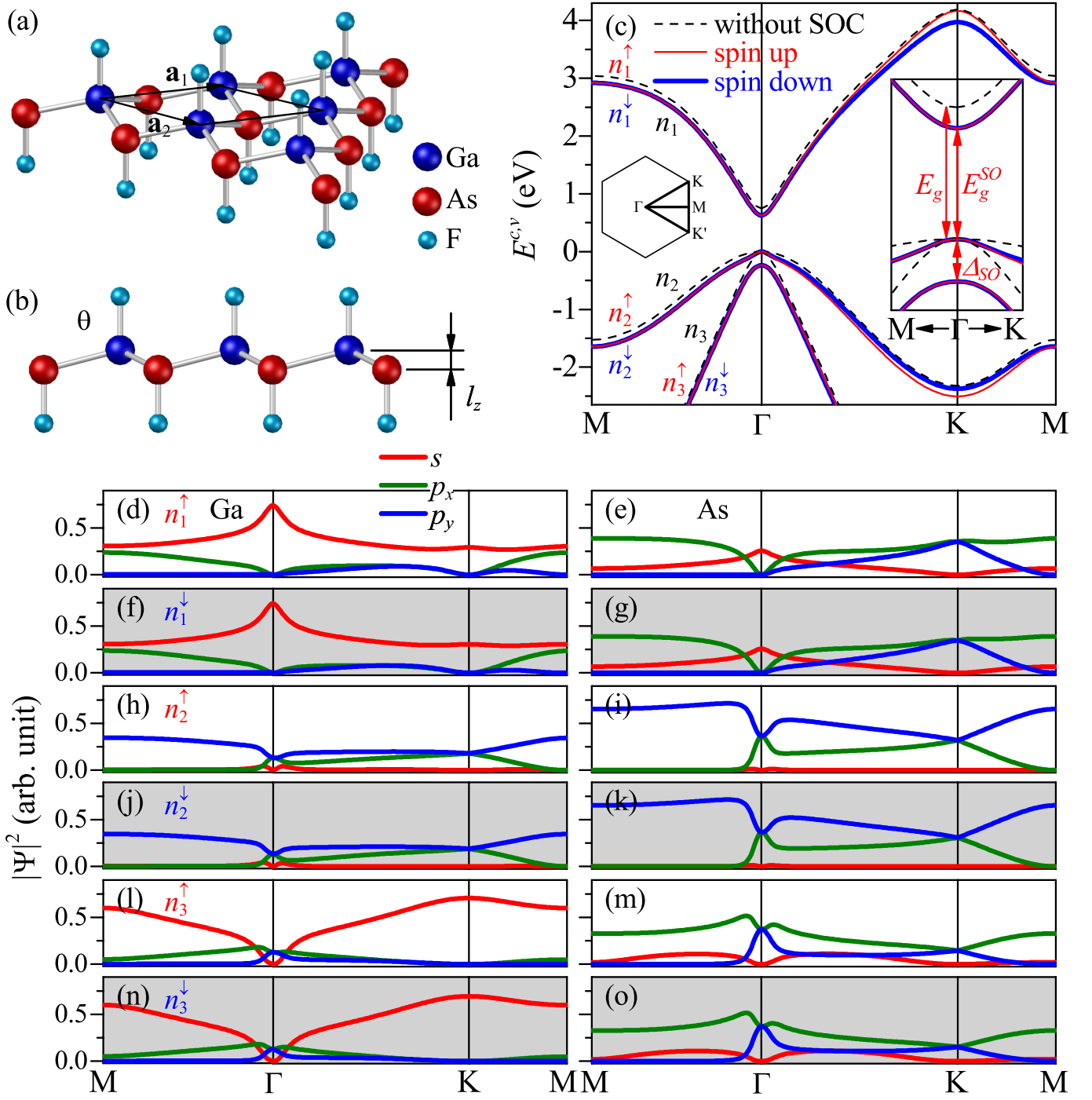


FIG. 1. (Color online) (a) Schematic representation of the monolayer GaAs decorated by F atoms. The unit cell is indicated by the rhombus. \mathbf{a}_1 and \mathbf{a}_2 are the two translation vectors. (b) Side view of the low-buckled monolayer GaAs with the buckling angle θ . (c) Spin-degenerate energy subbands without SOC (n_1 , n_2 , and n_3) and SOC-induced spin-polarized subbands (n_1^\uparrow , n_1^\downarrow , n_2^\uparrow , n_2^\downarrow , n_3^\uparrow , and n_3^\downarrow) along the high symmetry points. (d)–(o) State probabilities of various orbitals located at two sublattices Ga and As with spin-up (white zones) and spin-down (gray zones) arrangements. s , p_x , and p_y orbitals are indicated by red, green, and blue curves, respectively.

p_x -orbitals and minor p_y - and s -orbitals [Figs. 2(i) and (j)]. It is noteworthy that the Landau state reflects the average of accumulated neighboring zero-field electronic states with similar energies. In other words, the relative

strength among LL subenvelope function probabilities of various orbitals (or different sublattices) corresponds to the relative strength among zero-field probabilities of various orbitals (or different sublattices). In each LL group,

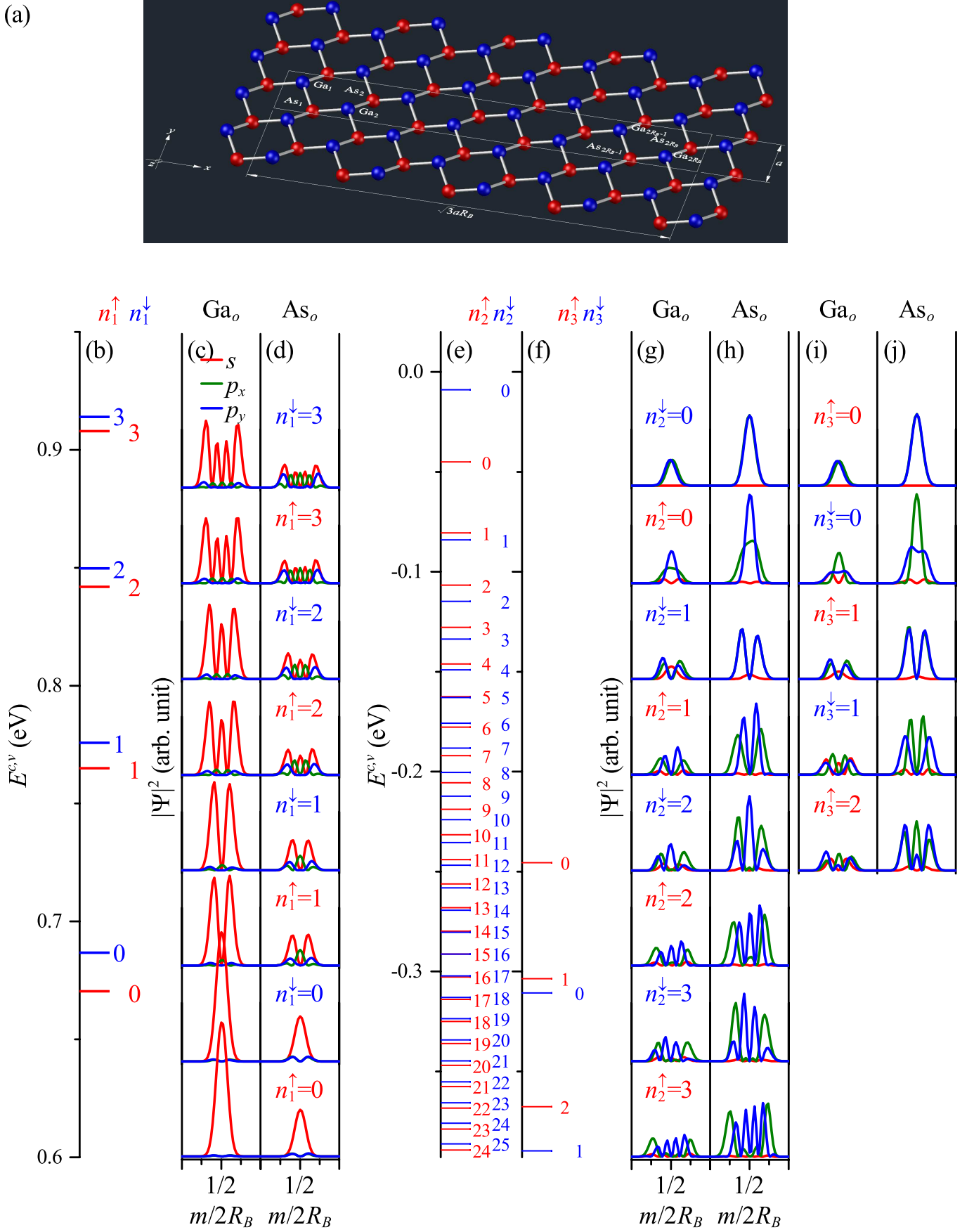


FIG. 2. (Color online) (a) Geometric structure of the low-buckled monolayer GaAs with an enlarged rectangular unit cell in $B_z \hat{z}$. (b)–(j) Spin-polarized LLs and the corresponding probabilities of the subenvelope functions near the localization center at $B_z = 60$ T.

the energy-dependent relative orbital strength is roughly associated with the \mathbf{k} -dependent relative orbital strength at $B_z = 0$ owing to the monotonously varying zero-field band structure near the Γ point. The dominated s -orbitals on the Ga sublattice have strength stronger than those on the As sublattice in the conduction LLs, and the increase of p_x - and p_y -orbital strength with the decrease of s -orbital strength take place as n_1^\uparrow and n_1^\downarrow grow [comparison between Figs. 2(c) and (d) and Figs. 1(d)–(g)]. Instead of the Ga sublattice, the dominated orbitals on the As sublattice in the valence LLs have larger strength. The p_x - and p_y -orbitals on a specific sublattice are of the same strength in the $n_2^\downarrow = 0$ and $n_3^\uparrow = 0$ valence LLs [Figs. 2(g) and (j)], reflecting the fact that the zero-field p_x - and p_y -orbitals have equivalent strength at the Γ point [Figs. 1(h)–(o)]. As the subband index increases, the $n_2^{\uparrow\downarrow}$ ($n_3^{\uparrow\downarrow}$) valence LLs become p_y -orbital- (p_x -orbital-) dominated, which resembles the \mathbf{k} -dependence of dominated orbitals near the Γ point. The aforementioned LL node regularities and energy-dependent orbital variation give a fundamental understanding for further researches in optical and transport properties, such as magneto-optical absorption selection rules including major/minor optical transitions and the possible/forbidden transport channels.

The low-lying LLs exhibit a spin-polarized B_z -dependent energy spectrum, as clearly shown in Fig. 3(a). All LLs have a monotonic variation to the magnetic field, which reflects the monotonic band structure near the Γ point at zero field. In each spin-up (or spin-down) LL subgroup, the energy spacing between LLs is enlarged when the magnetic field increases. The B_z dependence of the energy spacing is approximately linear owing to the parabolic energy dispersion at $B_z = 0$. Between the n th spin-up and spin-down LLs of the same group ($n_i^\uparrow = n_i^\downarrow = n$; $i \in \{1, 2, 3\}$), their energy spacing grows with the increment of B_z , arising from the enhanced SOC by the more localized LL wave functions. For instance, the spacing is 24 meV between $n_1^\uparrow = 0$ and $n_1^\downarrow = 0$ LLs at $B_z = 100$ T (comparable to the room temperature thermal energy). At small magnetic field ($B_z \rightarrow 0$), the energy spacing between the lowest conduction LL and the highest valence LL closes to the zero-field energy gap. For an increasing magnetic field, the gap gradually increases due to the rising of $n_1^\uparrow = 0$ LL state energy and the falling of $n_2^\downarrow = 0$ LL state energy. The DOS, defined as $\sum_{\mathbf{k}} \sum_{n_i^{\uparrow\downarrow}; i \in \{1, 2, 3\}} \delta[\omega - E^{c,v}(\mathbf{k}, n_i^{\uparrow\downarrow})]$, directly reflects the main features of the LL energy spectra as depicted in Fig. 3(b) [75, 76, 113]. Three groups of delta-function-like symmetric peaks respectively appear from ~ 0.62 eV, 0 eV, and -0.24 eV. The delta-function-like symmetric peaks have two-side-divergent structure at the peak frequency ω , i.e., the delta-function-like peak is symmetric about the axis of ω . Their peak heights are the same, indicating the identical degeneracy of LLs. In each spin-polarized LL subgroup, the peak spacing is shrunk for a larger subband index. The above-mentioned charac-

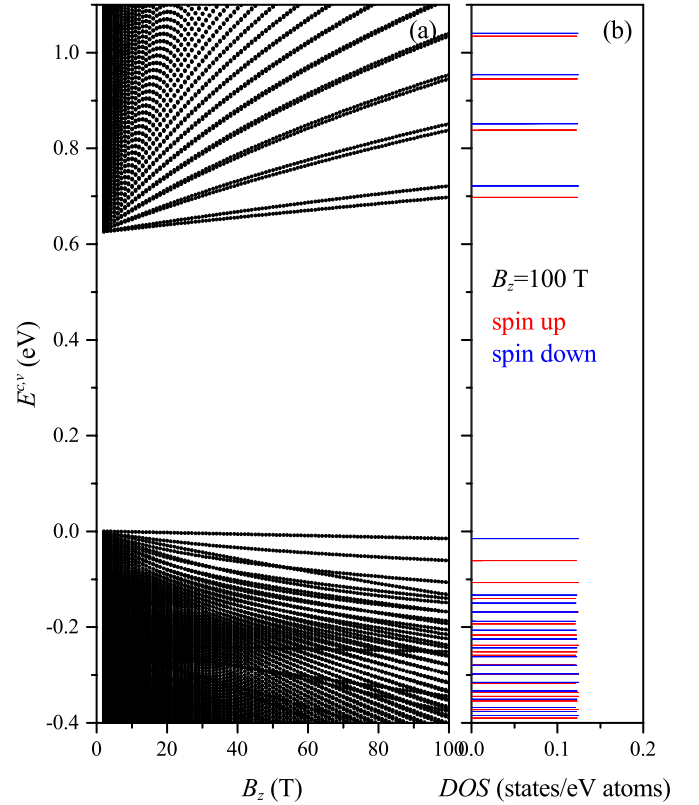


FIG. 3. (Color online) (a) Magnetic-field-dependent LL energy spectra of various groups. (b) Spin-polarized DOS at $B_z = 100$ T.

teristics of LL peaks, including peak structure, height, and spacing, can be verified through the experimental measurements using STS [10–14]. Furthermore, it is predicted that the optical absorption peaks are contributed by transitions between high-intensity-DOS LLs.

The magneto-electronic properties of monolayer GaAs with buckled structure, which are much different from those of monolayer graphene with planer structure, can be diversified by a perpendicular electric field, E_z . An electric potential difference $V_z = E_z l_z$ between the planes of Ga and As sublattice can cause monotonous/nonmonotonous dispersion relations, crossing LL spectra, enhancement of spin splitting, and modulation of energy gap. For a small magnetic field [Fig. 4(a)], the $n_1^{\uparrow\downarrow}$ and $n_2^{\downarrow}/n_3^{\uparrow\downarrow}$ LLs respectively exhibit monotonous decrease and increase as the electric field grows. An intergroup LL crossing takes place between $n_1^\uparrow = 0$ and $n_2^\downarrow = 0$ LLs at the critical electric field ($E_z^{cr} = 3.6$ V/Å), and their energy gap shrinks to zero (gray zone). Meanwhile, the spin splitting is enhanced, where the energy spacing between the $n_1^\uparrow = 0$ and $n_1^\downarrow = 0$ LLs is about 100 meV (larger than the room temperature thermal energy). For a large magnetic field [Fig. 4(b)], the $n_1^{\uparrow\downarrow}$ LLs present a monotonous decrease, while the $n_2^{\uparrow\downarrow}/n_3^{\uparrow\downarrow}$ LLs vary nonmonotonously with turning points (at $E_z \sim 4$ V/Å). The energy gap gradually shrinks and

reaches a minimum finite value without the intergroup crossing between $n_1^{\uparrow\downarrow}$ and $n_2^{\uparrow\downarrow}$ LLs. Magnetic fields can shift the gap of a top-gated monolayer GaAs. As the magnetic field grows over the critical strength [$B_z^{cr} \sim 18$ T in Fig. 4(c)], the gap is opened and then gradually increases.

The gap modulation owing to the competition between magnetic and electric fields is presented in detail by the color map, served as the E_z - B_z phase diagram [Fig. 4(d)]. There are four regions (I, II, III, and IV) separated by four boundaries (the critical curve, threshold line, threshold extension line, and finite minimum gap curve). The red critical curve with an upward trend indicates the critical electric and magnetic fields (E_z^{cr} and B_z^{cr}), where the system is a gapless semiconductor of $E_g^{SO} = 0$. The vertical threshold line at the maximum critical magnetic field, B_0^{cr} , figures out a drastic change of the gap between finite value and zero. The red critical curve and the vertical threshold line intersect at the critical point, $(B_0^{cr}, E_0^{cr}) = (70 \text{ T}, 5.3 \text{ V/\AA})$, indicating the maximum critical magnetic and electric fields. The curve on the right side of the critical point marks finite minimum gap during the competition. The semimetallic and semiconducting phases are respectively in regions I and (II, III, IV). Also, the electric field is in competition with the magnetic field, inducing complex responses to the gate voltage in various regions. For a specific magnetic field, the overlap between conduction and valence LLs in the region-I semimetal increases as the electric field grows. The gap of the region-II, region-III, and region-IV semiconductors respectively, shrinks to zero, decreases to a finite minimum value, and increases from a finite minimum value for a growing E_z . The diverse phase transitions occur from region I to regions (II, III, IV), e.g., a phase transition from semiconductor, gapless semiconductor to semimetal for regions II \rightarrow I, and a transition from semimetal to semiconductor for I \rightarrow IV. Abundant gap modulation can be achieved by controlling the external fields. The gate-voltage-controlled gap presents two types of modulation, associated to different region-to-region variations. [Fig. 4(e)]. At $B_z < B_0^{cr}$ (red and green curves), the E_z -dependent gap gradually shrinks to zero, where a large B_z corresponds to a large E_z^{cr} (cutoff points of the curves). At $B_z > B_0^{cr}$ (blue and magenta curves), the gap reduces to a finite value and then increases, where the red dashed curve shows the lower limit of such modulation and the finite minimum value grows with the increasing B_z . The ranges of gap modulation from regions II \rightarrow I and III \rightarrow IV are illustrated by the dark and light gray zones, respectively. The magnetic-field-controlled gap possesses three types of modulation [Fig. 4(f)]. At $E_z < E_{min}^{cr}$ (red curve), the B_z -dependent gap gradually increases (a variation from regions II \rightarrow III), where E_{min}^{cr} is the critical electric field at $B_z \rightarrow 0$. At $E_{min}^{cr} < E_z < E_0^{cr}$ (green curve), the gap is opened at E_z^{cr} and increases gradually from zero (from regions I \rightarrow II \rightarrow III). At $E_z > E_0^{cr}$ (blue curve), the opened gap gradually increases from a finite value at

B_0^{cr} (from regions I \rightarrow IV). The aforementioned external-field-controlled gap modulation and phase transitions are helpful in developing the top-gated electronic/optical devices and enable potential applications in phase-change electronic devices [114].

The main characteristics and the B_z - E_z -competition-induced modulation of symmetric Landau peaks in the DOS can be verified by STS. It is an extension of scanning tunneling microscopy (STM) [115–117] and provides detailed information about the DOS on a sample surface, such as silicon [118–120] and CNTs [121–124]. The tunneling differential conductance (dI/dV), proportional to the DOS [125], directly reveals the main characteristics, i.e., the structures, positions, and intensities of the peaks. Part of theoretical predictions on the LL energy spectra of few-layered graphene are verified, such as the $\sqrt{B_z}$ -dependent LLs in monolayer graphene [10–14], the linear B_z -dependent LLs in AB-stacked bilayer graphene [15–17], the concurrence of square-root and linear B_z -dependent LLs in graphene of trilayer ABA stacking [18]. The predicted magneto-electronic properties of the monolayer GaAs, including three groups of LLs with linear B_z -dependence, the external-field-controlled gap modulation and the SOC-induced spin splitting, could be further identified.

The aforementioned main features of wave functions can be confirmed by spectroscopic-imaging STM [126–128], which can resolve charge distributions from the local DOS and is an appropriate experimental technique for identifying standing waves and Landau wave functions on the surfaces of various condensed-matter systems. Standing waves have been directly observed at the surface steps of Au(111) and Cu(111) [126, 129], as well as finite-length metallic CNT [123, 130]. Also, the spatial mapping of the electronic states in the troughs between self-organized Pt nanowires on Ge(001) is presented [131, 132]. Recently, Landau orbits without nodes have been observed [133, 134], and subsequently, observations of the concentric-ring-like nodal structures have also been obtained [135, 136]. In monolayer GaAs, the predicted orbital domination for various groups of LLs and the relative strength of various orbitals (or different sublattices) for a specific LL could be examined through spectroscopic-imaging STM measurements on nodal structures.

Monolayer graphene and GaAs have much different essential properties and responses to external fields based on the orbital domination, SOC, and geometric structure. The low-energy electronic structure of planar graphene exhibits a pair of single-orbital-dominated (p_z) conduction/valence spin-degenerate subbands touching at the K point, resulting in a zero-gap. In contrast to the gapless semiconducting graphene, monolayer buckled GaAs possesses a direct energy gap at the Γ point among SOC-induced multi-orbital-dominated (s , p_x , and p_y) spin-polarized subbands, whose spin-splitting energies are \mathbf{k} -dependent. Distinct features are revealed in magnetic quantizations, such as the magnetic field dependence

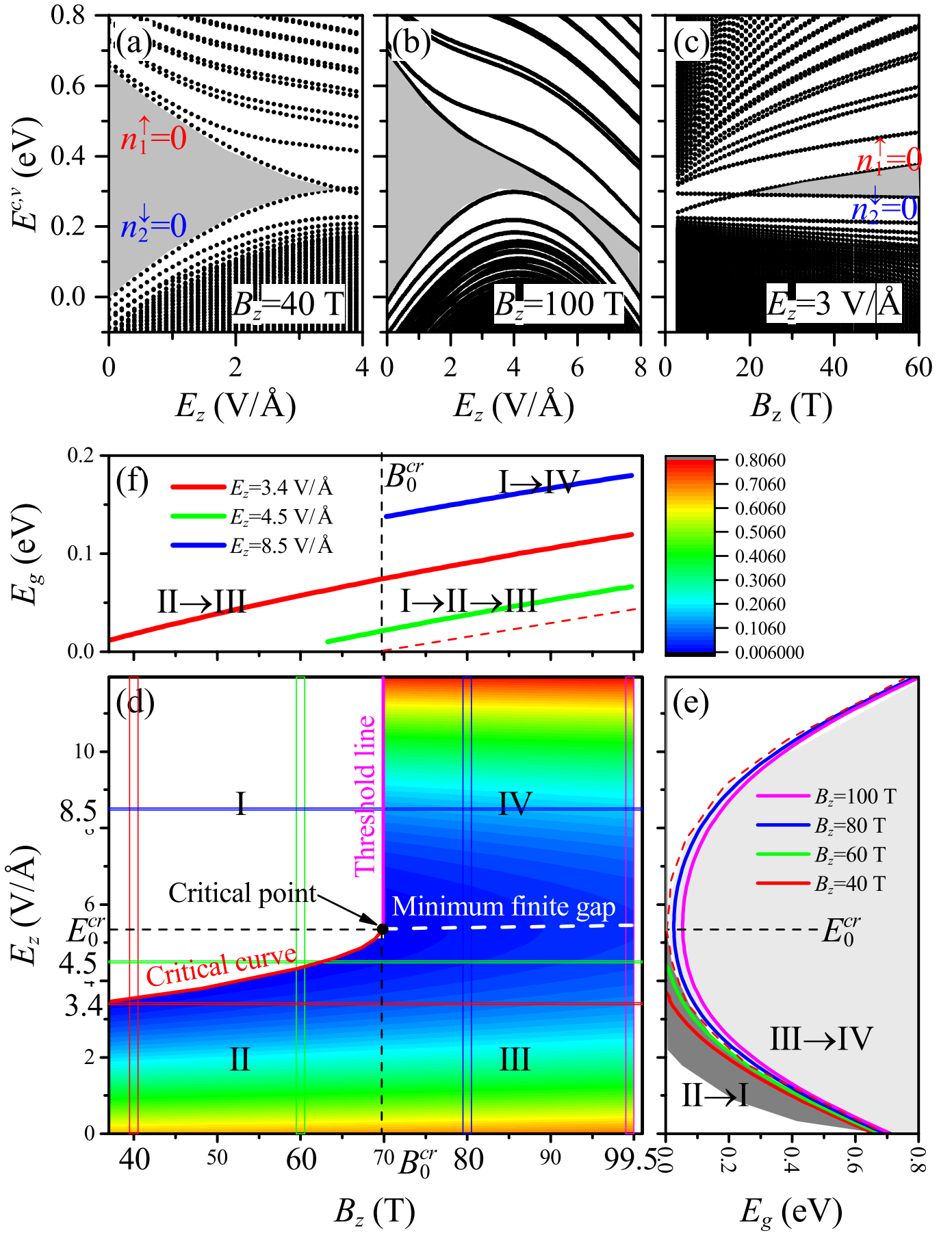


FIG. 4. (Color online) (a), (b) Gate-voltage-dependent LL energy spectra at $B_z = 40$ and 100 T. (c) Magnetic-field-dependent LL energy spectrum at $E_z = 3$ V/Å. (d)–(f) Dependence of energy gap on magnetic field and gate voltage.

of LLs, localization centers of Landau wave functions, and quantum mode regularities. The LLs reflect the main features of zero-field energy dispersions, exhibiting $\sqrt{B_z}$ -dependent spin-degenerate LLs and linear B_z -dependent spin-polarized LLs in monolayer graphene and GaAs, respectively. The localization centers of the spin-degenerate states (spin-polarized states) are at $1/6$, $2/6$, $4/6$, and $5/6$ (0 and $1/2$) positions of the enlarged unit cell. For a specific LL of graphene (GaAs), the major node numbers of subenvelope functions in different sublattices differ by one (are identical). Electric fields further cause an on-site energy difference between two distinct sublattices of GaAs with buckled structure, leading to the gap modulation, phase transition, and enhancement of spin splitting. The aforementioned differences clearly illustrate that electronic properties are diversified by the geometric structures, orbital hybridizations, spin configurations, as well as electric and magnetic fields.

IV. CONCLUSION

We develop the generalized tight-binding model to study the essential properties of monolayer GaAs. Many critical factors, including the buckled structure, multi-orbital hybridization, SOC, electric field, and magnetic field, are considered in the calculation simultaneously. This system in contrast to graphene is predicted to have rich and unique magnetic quantizations and phase transitions. The developed generalized tight-binding model provides a theoretical framework for investigating the competitions among various critical factors and affords systematic studies from multi-dimensional materials to hybrid systems. Theories with both single-particle and many-body schemes can also be combined to comprehend the essential physical properties, e.g., frequency-dependent and static Kubo formulas for exploring the optical absorption spectra [68, 75, 76, 111] and quantum Hall effect [arXiv:1704.01313], respectively.

Band structures and LLs of monolayer GaAs are very sensitive to the buckled structure, multi-orbital hybridizations, spin-orbital interactions, and external fields. Three groups of SOC-induced spin-polarized subbands ($n_1^{\uparrow\downarrow}$, $n_2^{\uparrow\downarrow}$, $n_3^{\uparrow\downarrow}$) initiated from the Γ point exhibit monotonous energy dispersions and strong \mathbf{k} -dependent spin splitting. There are a direct band gap ($E_g^{SO} = 0.623$ eV) between $n_1^{\uparrow\downarrow}$ and $n_2^{\uparrow\downarrow}$ subbands as well as a SOC-induced energy splitting ($\Delta_{SO} = 0.237$ eV) between $n_2^{\uparrow\downarrow}$ and $n_3^{\uparrow\downarrow}$ subbands at the Γ point. The whole-range state probabilities presenting the detailed orbital variations on different sublattices of various subbands are illustrated, showing that the conduction $n_1^{\uparrow\downarrow}$ subbands are s -orbital-dominated with larger state probabilities on the Ga sublattice; the valence $n_2^{\uparrow\downarrow}$ ($n_3^{\uparrow\downarrow}$) subbands are p_y -orbital- (p_x -orbital-) dominated with larger probabilities on the As sublattice. Magnetic quantization induces three groups of spin-polarized LLs with initial energies

respectively near 0.62 eV, 0 eV, and 0.24 eV and a gap of size $\sim E_g^{SO}$ between the lowest conduction and highest valence LLs, reflecting the energies of zero-field electronic states at the Γ point. Each LL is doubly degenerate based on one Γ valley and mirror symmetry. The LL energy spacing for any particular spin-polarized subgroup gradually shrinks as the state energy grows. The state probabilities of subenvelope functions are well-behaved in their spatial distributions, possessing oscillation patterns with regular nodes at the localization centers, similar to those of harmonic oscillators. The doubly degenerate spin-polarized LL states at $(k_x, k_y) = (0, 0)$ are localized at the 0 and $1/2$ positions of the enlarged unit cell, respectively. In each LL, the node numbers of various orbital subenvelope functions on the Ga and As sublattices are identical, and the s -orbital node number differs the p_x -orbital (p_y -orbital) node number by one. The orbital domination and the complex variation about the dominated/minor orbitals feature the average of accumulated neighboring zero-field electronic states, i.e., the energy-dependent relative orbital strength roughly corresponds to the \mathbf{k} -dependent relative orbital strength at $B_z = 0$ owing to the monotonous zero-field band structure near the Fermi level. These predicted characteristics of state probabilities could be examined through spectroscopic-imaging STM measurements on nodal structures.

The linear- B_z dependence of LL energies is revealed owing to the low-lying parabolic energy dispersions. For an increasing magnetic field, the gap is enlarged and the spin splitting is enhanced gradually. There are three groups of spin-polarized LL peaks in the DOS, directly reflects the main features of the LL energy spectra. The delta-function-like symmetric peak structure, initial frequencies for each group of LL peaks, degeneracy-related peak height, and shrunk frequency spacings for peaks of larger indices could be identified by the STS measurements.

The electric field, leading to an electric potential difference in the buckled structure, causes monotonous/nonmonotonous energy dispersions, LL crossing, enhancement of spin splitting, and gap modulation. For a small magnetic field $B_z < B_0^{cr}$, the intergroup LL crossing occurs between the conduction and valence LLs at the critical electric field, accompanied by the gap shrinkage and close; for a large magnetic field $B_z > B_0^{cr}$, the gap remains finite without the occurrence of intergroup LL crossing near the Fermi level. It should be noted that the spin splitting is enhanced with an energy spacing larger than the room temperature thermal energy. The complex gap modulations and phase transitions based on the competition between magnetic and electric fields are investigated. The E_z - B_z phase diagram illustrates the complex phase transitions between four characteristic regions. The E_z - (B_z -) controlled gap presents two (three) types of modulation, associated to different region-to-region variations. The field-controlled gap modulations and phase transitions are helpful in developing the top-gated electronic/optical devices and

phase-change electronic devices.

Monolayer GaAs, being 2D materials beyond graphene, is much different from graphene on the essential properties and responses to external fields owing to the orbital domination, SOC, and geometric structure. Distinct magnetic quantizations are revealed, such as the magnetic field dependence of LLs, localization centers of LL wave functions, and quantum mode regularities. Electric fields, leading to an on-site energy difference in GaAs with buckled structure, further induce the gap modulation, phase transition, and enhancement of spin splitting. The predicted magneto-electronic properties of the monolayer GaAs, including three groups of spin-polarized LLs with linear B_z -dependence, the external-field-controlled gap modulation/phase transition and the SOC-induced spin splitting, could be further experimentally identified by STS. Additionally, this work can be treated as a model study for compre-

hending magnetic quantizations of other group III-V 2D materials.

ACKNOWLEDGMENTS

We would like to thank all the contributors to this article for their valuable discussions and recommendations, especially Geng-Ming Hu, Matisse Wei-Yuan Tu, Ping-Yuan Lo, and Yu-Ming Wang. The authors thank Pei-Ju Chien for English discussions and corrections. One of us (Hsien-Ching Chung) thanks Ming-Hui Chung, Su-Ming Chen, Lien-Kuei Chien, Mi-Lee Kao, and Fu-Long Chen for financial support. This work was supported in part by the Gin Wen Town Printing Company, Taichung, Taiwan. This work was supported in part by the Ministry of Science and Technology of Taiwan under grant numbers MOST 105-2811-M-017-003, MOST 105-2112-M-017-002-MY2, and NSC 102-2112-M-006-007-MY3.

-
- [1] K. S. Novoselov, A. K. Geim, S. V. Morozov, D. Jiang, Y. Zhang, S. V. Dubonos, I. V. Grigorieva, and A. A. Firsov, *Science* **306**, 666 (2004).
 - [2] K. S. Novoselov, D. Jiang, F. Schedin, T. J. Booth, V. V. Khotkevich, S. V. Morozov, and A. K. Geim, *Proceedings of the National Academy of Sciences of the United States of America* **102**, 10451 (2005).
 - [3] C. Berger, Z. M. Song, X. B. Li, X. S. Wu, N. Brown, C. Naud, D. Mayou, T. B. Li, J. Hass, A. N. Marchenkov, E. H. Conrad, P. N. First, and W. A. de Heer, *Science* **312**, 1191 (2006).
 - [4] K. I. Bolotin, K. J. Sikes, Z. Jiang, M. Klima, G. Fudenberg, J. Hone, P. Kim, and H. L. Stormer, *Solid State Communications* **146**, 351 (2008).
 - [5] S. V. Morozov, K. S. Novoselov, M. I. Katsnelson, F. Schedin, D. C. Elias, J. A. Jaszczak, and A. K. Geim, *Physical Review Letters* **100**, 016602 (2008).
 - [6] A. A. Balandin, S. Ghosh, W. Z. Bao, I. Calizo, D. Teweldebrhan, F. Miao, and C. N. Lau, *Nano Letters* **8**, 902 (2008).
 - [7] R. R. Nair, P. Blake, A. N. Grigorenko, K. S. Novoselov, T. J. Booth, T. Stauber, N. M. R. Peres, and A. K. Geim, *Science* **320**, 1308 (2008).
 - [8] S. Bae, H. Kim, Y. Lee, X. F. Xu, J. S. Park, Y. Zheng, J. Balakrishnan, T. Lei, H. R. Kim, Y. I. Song, Y. J. Kim, K. S. Kim, B. Ozyilmaz, J. H. Ahn, B. H. Hong, and S. Iijima, *Nature Nanotechnology* **5**, 574 (2010).
 - [9] C. Lee, X. D. Wei, J. W. Kysar, and J. Hone, *Science* **321**, 385 (2008).
 - [10] G. Li, A. Luican, and E. Y. Andrei, *Physical Review Letters* **102**, 176804 (2009).
 - [11] D. L. Miller, K. D. Kubista, G. M. Rutter, M. Ruan, W. A. de Heer, P. N. First, and J. A. Stroscio, *Science* **324**, 924 (2009).
 - [12] Y. J. Song, A. F. Otte, Y. Kuk, Y. Hu, D. B. Torrance, P. N. First, W. A. de Heer, H. Min, S. Adam, M. D. Stiles, A. H. MacDonald, and J. A. Stroscio, *Nature* **467**, 185 (2010).
 - [13] A. Luican, G. H. Li, A. Reina, J. Kong, R. R. Nair, K. S. Novoselov, A. K. Geim, and E. Y. Andrei, *Physical Review Letters* **106**, 126802 (2011).
 - [14] W. X. Wang, L. J. Yin, J. B. Qiao, T. C. Cai, S. Y. Li, R. F. Dou, J. C. Nie, X. S. Wu, and L. He, *Physical Review B* **92**, 165420 (2015).
 - [15] E. A. Henriksen, Z. Jiang, L. C. Tung, M. E. Schwartz, M. Takita, Y. J. Wang, P. Kim, and H. L. Stormer, *Physical Review Letters* **100**, 087403 (2008).
 - [16] G. M. Rutter, S. Jung, N. N. Klimov, D. B. Newell, N. B. Zhitenev, and J. A. Stroscio, *Nature Physics* **7**, 649 (2011).
 - [17] L. J. Yin, Y. Zhang, J. B. Qiao, S. Y. Li, and L. He, *Physical Review B* **93**, 125422 (2016).
 - [18] L. J. Yin, S. Y. Li, J. B. Qiao, J. C. Nie, and L. He, *Physical Review B* **91**, 115405 (2015).
 - [19] F. Xia, D. B. Farmer, Y.-m. Lin, and P. Avouris, *Nano Letters* **10**, 715 (2010).
 - [20] G. R. Bhimanapati, Z. Lin, V. Meunier, Y. Jung, J. Cha, S. Das, D. Xiao, Y. Son, M. S. Strano, V. R. Cooper, L. B. Liang, S. G. Louie, E. Ringe, W. Zhou, S. S. Kim, R. R. Naik, B. G. Sumpter, H. Terrones, F. N. Xia, Y. L. Wang, J. Zhu, D. Akinwande, N. Alem, J. A. Schuller, R. E. Schaak, M. Terrones, and J. A. Robinson, *ACS Nano* **9**, 11509 (2015).
 - [21] F. Schwierz, J. Pezoldt, and R. Granzner, *Nanoscale* **7**, 8261 (2015).
 - [22] Y. B. Zhang, A. Rubio, and G. Le Lay, *Journal of Physics D-Applied Physics* **50**, 053004 (2017).
 - [23] L. Matthes, P. Gori, O. Pulci, and F. Bechstedt, *Physical Review B* **87**, 035438 (2013).
 - [24] W. Amamou, P. M. Odenthal, E. J. Bushong, D. J. O'Hara, Y. K. Luo, J. van Baren, I. Pinchuk, Y. Wu, A. S. Ahmed, J. Katoch, M. W. Bockrath, H. W. K. Tom, J. E. Goldberger, and R. K. Kawakami, *2d Materials* **2**, 035012 (2015).
 - [25] H. S. Liu, H. F. Feng, Y. Du, J. Chen, K. H. Wu, and J. J. Zhao, *2d Materials* **3**, 025034 (2016).
 - [26] H. Liu, A. T. Neal, Z. Zhu, Z. Luo, X. F. Xu, D. Tomanek, and P. D. Ye, *ACS Nano* **8**, 4033 (2014).

- [27] L. K. Li, Y. J. Yu, G. J. Ye, Q. Q. Ge, X. D. Ou, H. Wu, D. L. Feng, X. H. Chen, and Y. B. Zhang, *Nature Nanotechnology* **9**, 372 (2014).
- [28] J. O. Island, G. A. Steele, H. S. J. van der Zant, and A. Castellanos-Gomez, *2D Materials* **2**, 011002 (2015).
- [29] H. Sahin, S. Cahangirov, M. Topsakal, E. Bekaroglu, E. Akturk, R. T. Senger, and S. Ciraci, *Physical Review B* **80**, 155453 (2009).
- [30] H. L. L. Zhuang, A. K. Singh, and R. G. Hennig, *Physical Review B* **87**, 165415 (2013).
- [31] F. C. Chuang, L. Z. Yao, Z. Q. Huang, Y. T. Liu, C. H. Hsu, T. Das, H. Lin, and A. Bansil, *Nano Letters* **14**, 2505 (2014).
- [32] Q. H. Wang, K. Kalantar-Zadeh, A. Kis, J. N. Coleman, and M. S. Strano, *Nature Nanotechnology* **7**, 699 (2012).
- [33] C. Ataca, H. Sahin, and S. Ciraci, *Journal of Physical Chemistry C* **116**, 8983 (2012).
- [34] D. Jariwala, V. K. Sangwan, L. J. Lauhon, T. J. Marks, and M. C. Hersam, *ACS Nano* **8**, 1102 (2014).
- [35] G. Plechinger, A. Castellanos-Gomez, M. Buscema, H. S. J. van der Zant, G. A. Steele, A. Kuc, T. Heine, C. Schuller, and T. Korn, *2D Materials* **2**, 015006 (2015).
- [36] C. C. Liu, W. X. Feng, and Y. G. Yao, *Physical Review Letters* **107**, 076802 (2011).
- [37] C. C. Liu, H. Jiang, and Y. G. Yao, *Physical Review B* **84**, 195430 (2011).
- [38] Y. Xu, B. H. Yan, H. J. Zhang, J. Wang, G. Xu, P. Z. Tang, W. H. Duan, and S. C. Zhang, *Physical Review Letters* **111**, 136804 (2013).
- [39] P. Vogt, P. De Padova, C. Quaresima, J. Avila, E. Frantzeskakis, M. C. Asensio, A. Resta, B. Ealet, and G. Le Lay, *Physical Review Letters* **108**, 155501 (2012).
- [40] L. Chen, C. C. Liu, B. J. Feng, X. Y. He, P. Cheng, Z. J. Ding, S. Meng, Y. G. Yao, and K. H. Wu, *Physical Review Letters* **109**, 056804 (2012).
- [41] L. Tao, E. Cinquanta, D. Chiappe, C. Grazianetti, M. Fanciulli, M. Dubey, A. Molle, and D. Akinwande, *Nature Nanotechnology* **10**, 227 (2015).
- [42] P. De Padova, A. Generosi, B. Paci, C. Ottaviani, C. Quaresima, B. Olivieri, E. Salomon, T. Angot, and G. Le Lay, *2D Materials* **3**, 031011 (2016).
- [43] L. Meng, Y. L. Wang, L. Z. Zhang, S. X. Du, R. T. Wu, L. F. Li, Y. Zhang, G. Li, H. T. Zhou, W. A. Hofer, and H. J. Gao, *Nano Letters* **13**, 685 (2013).
- [44] A. Fleurence, R. Friedlein, T. Ozaki, H. Kawai, Y. Wang, and Y. Yamada-Takamura, *Physical Review Letters* **108**, 245501 (2012).
- [45] L. F. Li, S. Z. Lu, J. B. Pan, Z. H. Qin, Y. Q. Wang, Y. L. Wang, G. Y. Cao, S. X. Du, and H. J. Gao, *Advanced Materials* **26**, 4820 (2014).
- [46] M. Derivaz, D. Dentel, R. Stephan, M. C. Hanf, A. Mehdaoui, P. Sonnet, and C. Pirri, *Nano Letters* **15**, 2510 (2015).
- [47] M. E. Davila, L. Xian, S. Cahangirov, A. Rubio, and G. Le Lay, *New Journal of Physics* **16**, 095002 (2014).
- [48] F.-F. Zhu, W.-J. Chen, Y. Xu, C.-L. Gao, D.-D. Guan, C.-H. Liu, D. Qian, S.-C. Zhang, and J.-F. Jia, *Nature Materials* **14**, 1020 (2015).
- [49] A. Acun, L. Zhang, P. Bampoulis, M. Farmanbar, A. van Houselt, A. N. Rudenko, M. Lingenfelder, G. Brocks, B. Poelsema, M. I. Katsnelson, and H. J. W. Zandvliet, *Journal of Physics-Condensed Matter* **27**, 443002 (2015).
- [50] C. J. Tabert and E. J. Nicol, *Physical Review B* **88**, 085434 (2013).
- [51] V. Y. Tsaran and S. G. Sharapov, *Physical Review B* **90**, 205417 (2014).
- [52] S. Y. A. Yang, H. Pan, and F. Zhang, *Rsc Advances* **5**, 83350 (2015).
- [53] S. C. Chen, C. L. Wu, J. Y. Wu, and M. F. Lin, *Physical Review B* **94**, 045410 (2016).
- [54] J. Y. Wu, S. C. Chen, G. Gumbs, and M. F. Lin, *Physical Review B* **94**, 205427 (2016).
- [55] C. L. Lin, R. Arafune, K. Kawahara, M. Kanno, N. Tsukahara, E. Minamitani, Y. Kim, M. Kawai, and N. Takagi, *Physical Review Letters* **110**, 076801 (2013).
- [56] R. R. Nair, W. C. Ren, R. Jalil, I. Riaz, V. G. Kravets, L. Britnell, P. Blake, F. Schedin, A. S. Mayorov, S. J. Yuan, M. I. Katsnelson, H. M. Cheng, W. Strupinski, L. G. Bulusheva, A. V. Okotrub, I. V. Grigorieva, A. N. Grigorenko, K. S. Novoselov, and A. K. Geim, *Small* **6**, 2877 (2010).
- [57] J. T. Robinson, J. S. Burgess, C. E. Junkermeier, S. C. Badescu, T. L. Reinecke, F. K. Perkins, M. K. Zalalutdinov, J. W. Baldwin, J. C. Culbertson, P. E. Sheehan, and E. S. Snow, *Nano Letters* **10**, 3001 (2010).
- [58] K. J. Jeon, Z. Lee, E. Pollak, L. Moreschini, A. Bostwick, C. M. Park, R. Mendelsberg, V. Radmilovic, R. Kostecki, T. J. Richardson, and E. Rotenberg, *ACS Nano* **5**, 1042 (2011).
- [59] C. Si, J. W. Liu, Y. Xu, J. Wu, B. L. Gu, and W. H. Duan, *Physical Review B* **89**, 115429 (2014).
- [60] S. M. Sze and J. C. Irvin, *Solid-State Electronics* **11**, 599 (1968).
- [61] N. D. Arora, J. R. Hauser, and D. J. Roulston, *IEEE Transactions on Electron Devices* **29**, 292 (1982).
- [62] M. W. Zhao, X. Chen, L. Y. Li, and X. M. Zhang, *Scientific Reports* **5**, 8441 (2015).
- [63] P. R. Wallace, *Physical Review* **71**, 622 (1947).
- [64] C. P. Chang, C. L. Lu, F. L. Shyu, R. B. Chen, Y. C. Huan, and M. F. Lin, *Carbon* **43**, 1424 (2005).
- [65] R. B. Chen, C. W. Chiu, and M. F. Lin, *RSC Advances* **5**, 53736 (2015).
- [66] J. H. Ho, Y. H. Lai, Y. H. Chiu, and M. F. Lin, *Physica E* **40**, 1722 (2008).
- [67] Y. H. Lai, J. H. Ho, C. P. Chang, and M. F. Lin, *Physical Review B* **77**, 085426 (2008).
- [68] C.-Y. Lin, J.-Y. Wu, Y.-J. Ou, Y.-H. Chiu, and M.-F. Lin, *Physical Chemistry Chemical Physics* **17**, 26008 (2015).
- [69] H.-C. Wu, A. N. Chaika, T.-W. Huang, A. Syrlybekov, M. Abid, V. Y. Aristov, O. V. Molodtsova, S. V. Babenkov, D. Marchenko, J. Sanchez-Barriga, P. S. Mandal, A. Y. Varykhalov, Y. Niu, B. E. Murphy, S. A. Krasnikov, O. Luebben, J. J. Wang, H. Liu, L. Yang, H. Zhang, M. Abid, Y. T. Janabi, S. N. Molotkov, C.-R. Chang, and I. Shvets, *ACS Nano* **9**, 8967 (2015).
- [70] H. C. Wu, A. N. Chaika, M. C. Hsu, T. W. Huang, M. Abid, V. Y. Aristov, O. V. Molodtsova, S. V. Babenkov, Y. R. Niu, B. E. Murphy, S. A. Krasnikov, O. Lubben, H. J. Liu, B. S. Chun, Y. T. Janabi, S. N. Molotkov, I. V. Shvets, A. I. Lichtenstein, M. I. Katsnelson, and C. R. Chang, *Nature Communications* **8**, 14453 (2017).
- [71] M. Fujita, K. Wakabayashi, K. Nakada, and K. Kusakabe, *Journal of the Physical Society of Japan* **65**, 1920

- (1996).
- [72] K. Wakabayashi, M. Fujita, H. Ajiki, and M. Sigrist, *Physical Review B* **59**, 8271 (1999).
 - [73] H. C. Chung, Y. C. Huang, M. H. Lee, C. C. Chang, and M. F. Lin, *Physica E* **42**, 711 (2010).
 - [74] H.-C. Chung, M.-H. Lee, C.-P. Chang, Y.-C. Huang, and M.-F. Lin, *Journal of the Physical Society of Japan* **80**, 044602 (2011).
 - [75] H.-C. Chung, C.-P. Chang, C.-Y. Lin, and M.-F. Lin, *Physical Chemistry Chemical Physics* **18**, 7573 (2016).
 - [76] H. C. Chung, Y. T. Lin, S. Y. Lin, C. H. Ho, C. P. Chang, and M. F. Lin, *Carbon* **109**, 883 (2016).
 - [77] R. Saito, M. Fujita, G. Dresselhaus, and M. S. Dresselhaus, *Physical Review B* **46**, 1804 (1992).
 - [78] M. F. Lin and K. W. K. Shung, *Physical Review B* **50**, 17744 (1994).
 - [79] M. F. Lin and K. W. K. Shung, *Physical Review B* **52**, 8423 (1995).
 - [80] C. L. Kane and E. J. Mele, *Physical Review Letters* **78**, 1932 (1997).
 - [81] S. Roche, G. Dresselhaus, M. S. Dresselhaus, and R. Saito, *Physical Review B* **62**, 16092 (2000).
 - [82] F. L. Shyu, C. P. Chang, R. B. Chen, C. W. Chiu, and M. F. Lin, *Physical Review B* **67**, 045405 (2003).
 - [83] K. Szalowski, *Carbon* **118**, 78 (2017).
 - [84] L. Zhang, B.-C. Lin, Y.-F. Wu, H. Wu, T.-W. Huang, C.-R. Chang, X. Ke, M. Kurttepli, G. V. Tendeloo, J. Xu, D. Yu, and Z.-M. Liao, *ACS Nano* **0**, null (0), <http://dx.doi.org/10.1021/acsnano.7b02494>.
 - [85] J. Y. Wu, S. C. Chen, and M. F. Lin, *New Journal of Physics* **16**, 125002 (2014).
 - [86] J. Y. Wu, C. Y. Lin, G. Gumbs, and M. F. Lin, *RSC Advances* **5**, 51912 (2015).
 - [87] Y. Takao, H. Asahina, and A. Morita, *Journal of the Physical Society of Japan* **50**, 3362 (1981).
 - [88] Y. Takao and A. Morita, *Physica B and C* **105**, 93 (1981).
 - [89] E. T. Sisakht, M. H. Zare, and F. Fazileh, *Physical Review B* **91**, 085409 (2015).
 - [90] J. Y. Wu, S. C. Chen, G. Gumbs, and M. F. Lin, *Physical Review B* **95**, 115411 (2017).
 - [91] E. Cappelluti, R. Roldan, J. A. Silva-Guillen, P. Ordejon, and F. Guinea, *Physical Review B* **88**, 075409 (2013).
 - [92] F. Zahid, L. Liu, Y. Zhu, J. Wang, and H. Guo, *Aip Advances* **3**, 052111 (2013).
 - [93] Y. H. Ho, Y. H. Wang, and H. Y. Chen, *Physical Review B* **89**, 155316 (2014).
 - [94] Y. H. Ho, C. W. Chiu, W. P. Su, and M. F. Lin, *Applied Physics Letters* **105**, 222411 (2014).
 - [95] E. Ridolfi, D. Le, T. S. Rahman, E. R. Mucciolo, and C. H. Lewenkopf, *Journal of Physics-Condensed Matter* **27**, 365501 (2015).
 - [96] Y. H. Ho, W. P. Su, and M. F. Lin, *RSC Advances* **5**, 20858 (2015).
 - [97] J. C. Slater and G. F. Koster, *Physical Review* **94**, 1498 (1954).
 - [98] P. Vogl, H. P. Hjalmarson, and J. D. Dow, *Journal of Physics and Chemistry of Solids* **44**, 365 (1983).
 - [99] I. Zutic, J. Fabian, and S. Das Sarma, *Reviews of Modern Physics* **76**, 323 (2004).
 - [100] R. Peierls, *Z. Phys.* **80**, 763 (1933).
 - [101] F. London, *Superfluids, Vol. 1: Macroscopic Theory of Superconductivity* (John Wiley & Sons, New York, 1950) p. 152.
 - [102] L. Onsager, in *Proceedings of the International Conference on Theoretical Physics, Kyoto and Tokyo, September, 1953* (Science Council of Japan, Tokyo, 1954) p. 935.
 - [103] S. Giglberger, L. E. Golub, V. V. Bel'kov, S. N. Danilov, D. Schuh, C. Gerl, F. Rohlfing, J. Stahl, W. Wegscheider, D. Weiss, W. Prettl, and S. D. Ganichev, *Physical Review B* **75**, 035327 (2007).
 - [104] Y. A. Bychkov and E. I. Rashba, *Journal of Physics C-Solid State Physics* **17**, 6039 (1984).
 - [105] E. Schrodinger, *Physical Review* **28**, 1049 (1926).
 - [106] M. W. Y. Tu and W.-M. Zhang, *Physical Review B* **78**, 235311 (2008).
 - [107] P. M. Perez-Piskunow, G. Usaj, C. A. Balseiro, and L. E. F. Foà Torres, *Physical Review B* **89**, 121401 (2014).
 - [108] G. Usaj, P. M. Perez-Piskunow, L. E. F. Foà Torres, and C. A. Balseiro, *Physical Review B* **90**, 115423 (2014).
 - [109] H.-C. Chung, P.-H. Yang, T.-S. Li, and M.-F. Lin, *Philosophical Magazine* **94**, 1859 (2014).
 - [110] H.-C. Chung, W.-P. Su, and M.-F. Lin, *Physical Chemistry Chemical Physics* **15**, 868 (2013).
 - [111] H. C. Chung, M. H. Lee, C. P. Chang, and M. F. Lin, *Optics Express* **19**, 23350 (2011).
 - [112] V. A. Saroka, M. V. Shuba, and M. E. Portnoi, *Physical Review B* **95**, 155438 (2017).
 - [113] P.-Y. Lo, H.-N. Xiong, and W.-M. Zhang, *Scientific Reports* **5**, 9423 (2015).
 - [114] Y. Li, K. A. N. Duerloo, K. Wauson, and E. J. Reed, *Nature Communications* **7**, 10671 (2016).
 - [115] G. Binning, H. Rohrer, C. Gerber, and E. Weibel, *Physical Review Letters* **49**, 57 (1982).
 - [116] G. Binnig and H. Rohrer, *Helvetica Physica Acta* **55**, 726 (1982).
 - [117] G. Binnig, H. Rohrer, C. Gerber, and E. Weibel, *Physical Review Letters* **50**, 120 (1983).
 - [118] R. J. Hamers, R. M. Tromp, and J. E. Demuth, *Physical Review Letters* **56**, 1972 (1986).
 - [119] R. M. Feenstra, J. A. Stroscio, and A. P. Fein, *Surface Science* **181**, 295 (1987).
 - [120] M. N. Piancastelli, N. Motta, A. Sgarlata, A. Balzarotti, and M. Decrescenzi, *Physical Review B* **48**, 17892 (1993).
 - [121] J. W. G. Wildoer, L. C. Venema, A. G. Rinzi, R. E. Smalley, and C. Dekker, *Nature* **391**, 59 (1998).
 - [122] P. Kim, T. W. Odom, J. L. Huang, and C. M. Lieber, *Physical Review Letters* **82**, 1225 (1999).
 - [123] L. C. Venema, J. W. G. Wildoer, J. W. Janssen, S. J. Tans, H. Tuinstra, L. P. Kouwenhoven, and C. Dekker, *Science* **283**, 52 (1999).
 - [124] L. C. Venema, J. W. Janssen, M. R. Buitelaar, J. W. G. Wildoer, S. G. Lemay, L. P. Kouwenhoven, and C. Dekker, *Physical Review B* **62**, 5238 (2000).
 - [125] J. Tersoff and D. R. Hamann, *Physical Review B* **31**, 805 (1985).
 - [126] M. F. Crommie, C. P. Lutz, and D. M. Eigler, *Science* **262**, 218 (1993).
 - [127] S. Ilani, J. Martin, E. Teitelbaum, J. H. Smet, D. Mahalu, V. Umansky, and A. Yacoby, *Nature* **427**, 328 (2004).
 - [128] A. Richardella, P. Roushan, S. Mack, B. Zhou, D. A. Huse, D. D. Awschalom, and A. Yazdani, *Science* **327**,

- 665 (2010).
- [129] M. F. Crommie, C. P. Lutz, and D. M. Eigler, *Nature* **363**, 524 (1993).
 - [130] J. Lee, S. Eggert, H. Kim, S. J. Kahng, H. Shinohara, and Y. Kuk, *Physical Review Letters* **93**, 166403 (2004).
 - [131] A. van Houselt, N. Oancel, B. Poelsema, and H. J. W. Zandvliet, *Nano Letters* **6**, 1439 (2006).
 - [132] R. Heimbuch, A. van Houselt, M. Farmanbar, G. Brocks, and H. J. W. Zandvliet, *Journal of Physics-Condensed Matter* **25**, 014014 (2013).
 - [133] K. Hashimoto, C. Sohrmann, J. Wiebe, T. Inaoka, F. Meier, Y. Hirayama, R. A. Roemer, R. Wiesendanger, and M. Morgenstern, *Physical Review Letters* **101**, 256802 (2008).
 - [134] D. L. Miller, K. D. Kubista, G. M. Rutter, M. Ruan, W. A. de Heer, M. Kindermann, P. N. First, and J. A. Stroscio, *Nature Physics* **6**, 811 (2010).
 - [135] K. Hashimoto, T. Champel, S. Florens, C. Sohrmann, J. Wiebe, Y. Hirayama, R. A. Roemer, R. Wiesendanger, and M. Morgenstern, *Physical Review Letters* **109**, 116805 (2012).
 - [136] Y.-S. Fu, M. Kawamura, K. Igarashi, H. Takagi, T. Hanaguri, and T. Sasagawa, *Nature Physics* **10**, 815 (2014).